IEEE Access
Multidisciplinary | Rapid Review | Open Access Journal

Received May 23, 2019, accepted July 3, 2019, date of publication July 9, 2019, date of current version July 29, 2019.

Digital Object Identifier 10.1109/ACCESS.2019.2927501

A comparison of the Long Working Distance of the GRIN Lens- and C-Lens-Based OCT Probe

YINGWEI FAN[1], SITE LUO[2,3], AND HONGXIANG KANG[1]
[1]Beijing Institute of Radiation Medicine, Beijing 100850, China
[2]WiseViewer Technology Company Ltd, Shenzhen 518000, China
[3]Department of Electrical Engineering, Tsinghua University, Beijing 100084, China

Corresponding authors: Site Luo (lost147258@163.com) and Hongxiang Kang (khx007@163.com)

This work was supported in part by the China Postdoctoral Science Foundation under Grant 2018M643846.

ABSTRACT The standard technical scheme for imaging with an endoscopic optical coherence tomography (OCT) probe is to use a GRIN lens to focus the beam. However, when a long working distance is required of the OCT probe, various factors will affect the imaging quality. Here, we conduct a theoretical calculation to analyze the sensitivity of the GRIN lens and the C-lens of an OCT probe. The sensitivity of $\omega_0 V_s L$ of the GRIN lens is ten times higher than that of the C-lens. The sensitivity of $Z_0 V_s L$ of the GRIN lens is 24 times higher than that of the C-lens. In addition, the sensitivity of the radius of curvature of the C-lens is compared with the sensitivity of the length of the GRIN lens, and the sensitivity for the GRIN lens is about five times higher than the sensitivity of the radius of curvature for the C-lens. Furthermore, fabricating a C-lens-based OCT probe is much cheaper than a GRIN-lens-based one. Hence, our calculations suggest that the C-lens is a better choice for a long-working-distance OCT probe.

INDEX TERMS Optical coherence tomography, endoscopic probe, working distance, GRIN lens, C-lens.

I. INTRODUCTION

OCT is a useful tool for imaging biological tissues [1],[2]. The first reported miniaturized OCT probes are circumferential scanning probes, which use a gradient-index (GRIN) lens to focus the light emitted from the fiber, and a small prism connected to the GRIN lens deflects the light onto the tissue [3]. GRIN lenses commonly have a tiny diameter and flat surfaces at both ends, which is helpful for creating high quality joints between the lens and the prism. The assembling procedure plays a very important role in an accurate probe design. The fabrication of optical probes with specific design parameters relies on high precision probe components [4]. However, circumferential scanning can also be obtained by distally rotating a prism with a micro-motor to scan the light beam in a direction perpendicular to the axis of the imaging probe, and the prism is apart from the GRIN lens so that the flat ends of the optical components are not necessary [5]–[7]. Side scanning probes are usually based on MEMS scanning mirrors to achieve two-dimensional (2D) optical scans [8]–[10]. All reported OCT probes are exclusively based on GRIN lenses and commonly have small imaging areas due to the short working distances [8]–[13]. Duan *et al.* demonstrated that the longest working distance of a 0.27-pitch (1.955 mm) GRIN lens (n = 1.6164 and g = 0.8521 mm^{-1}) is 5 mm [14]. Circumferential scanning OCT probes are extensively applied for imaging hollow organs [15], [16]. However, OCT imaging of a large lumen brings extra challenges, such as the human esophagus and colon. OCT probes have to achieve a greater than 10 mm working distance because the diameter of the esophagus is approximately 20-25 mm [17],[18]. Circumferential scanning probes for esophageal OCT images have been demonstrated by some research groups that designed a long working distance [19],[20]. Kang *et al.* reported an OCT probe with a 9 mm working distance and balloon-based catheters to provide a real-time surveillance tool for cases of Barrett's esophagus (BE) [21].

However, designing and fabricating an OCT probe with a greater than 10 mm working distance is a great challenge. Wang *et al.* report a numerical simulation about an OCT probe with an 11.25 mm working distance based on a GRIN lens length of 0.7 mm (g = 1.372) [22]. Jung W *et al.* did extensive and elaborate numerical simulations about GRIN lens-based OCT probes with a goal of achieving a single GRIN lens-based probe with a longer working distance and a smaller beam radius by using a longer spacer and an

The associate editor coordinating the review of this manuscript and approving it for publication was Vishal Srivastava.

extremely short-pitch GRIN lens. The simulation showed that the GRIN lens should be selected to be extremely short with a pitch under 0.045 [23]. Furthermore, the space between the fiber and the GRIN lens should be more than 7.8 mm, which will result in a large GRIN lens diameter, which contradicts the goal of an endoscopic small size design [23]. So the reported long-working-distance OCT probes based on GRIN lenses all used a compound lens method. Li *et al.* reported an OCT imaging catheter with a 39 μm spot size at a 9 mm working distance utilizing compounded optical elements of a glass rod and two GRIN lenses [24],[25]. However, the fabrication procedure is very complicated. The sensitivity of the working distance and beam diameter to the length of the GRIN lens is very high, and the tolerance of the length should be less than 10 μm.

GRIN lenses are the most common optical components for the construction of miniaturized OCT probes [23]-[25]. Commercial GRIN lenses (0.23-0.29 pitch) have a short working distance (less than 6 mm) and a small beam spot size [14]. The longer working distance ($\sim$10 mm) can be achieved by utilizing an extremely short GRIN lens (0.04-0.05 pitch) and multiple GRIN lens [25]. That signifies processing a GRIN rod with a length of 0.5 mm and a tolerance of 10 μm. Both the ultra-short GRIN lens and a compound lens bring great challenges to the processing and assembly of the probe. The processed procedure is so complicated that the rate of production for finished products is very limited. In contrast, C-lenses also are rod lenses, which are widely used in optical communications, which commonly have a longer working distance. In our previous research, a miniature OCT probes can be constructed with low-cost C-lenses and reach long working distances [26],[27]. Recently, an elegant research demonstrates that nano-optic OCT endoscopic probe has been developed and is used into imaging the human lung tissue specimens *ex vivo* and the pulmonary airways of sheep *in vivo* [28]. The working distance of this endoscopic probe is set as 0.5 mm. However, the long-working-distance analysis is not be reached.

An OCT probe contains numerous trade-offs between the working distance and the spot size. In this study, we set a trade-off standard with a 10 mm working distance and a 50 μm spot size. Exhaustive numerical simulations are calculated to compare the differences between the GRIN-lens-based catheter and the C-lens-based catheter.

II. METHOD

The output beam from a GRIN lens' or a C-lens' rear end is considered to be a Gaussian beam. For a GRIN lens, n is the refractive index of the GRIN lens at the center, g is the gradient constant of the GRIN lens, and L is the length of the GRIN lens. For a C-lens, n is the refractive index, r is the radius of curvature of the rear surface, and L is the length of the C-lens. The diameter of a GRIN lens and a C-lens rod is D. The distance between the fiber end and the lens' front end is defined as b, and this space is filled with air whose refractive index (n_0) is 1. The position from the rear surface of a GRIN lens or a C-lens is z, and the spot diameter at position z is defined as ω.

The lateral resolution of a probe is determined by the beam waist, which is the spot diameter on the focal plane. The spot diameter at the beam waist is defined as $2\omega_0$, so the spot radius is ω_0. The distance between the rear surface of a GRIN lens or a C-lens and the focal plane is defined as Z_0. The parameters of the beam (i.e., z, ω, ω_0 and Z_0) can be calculated with an ABCD matrix based on b and the parameters of a GRIN lens (i.e., n, g, L) or C-lens (i.e., n, r, L).

The ABCD matrix of a fiber-coupling-focus module based on a GRIN lens is given by Eq (1), and the calculation details can be found in Ref [12].

$$\begin{bmatrix} A & B \\ C & D \end{bmatrix} = \begin{bmatrix} 1 & z \\ 0 & 1 \end{bmatrix} \begin{bmatrix} 1 & 0 \\ 0 & n \end{bmatrix} \begin{bmatrix} \cos(gL) & \frac{1}{g}\sin(gL) \\ -g\sin(gL) & \cos(gL) \end{bmatrix} \times \begin{bmatrix} 1 & 0 \\ 0 & \frac{1}{n} \end{bmatrix} \begin{bmatrix} 1 & b \\ 0 & 1 \end{bmatrix} \quad (1)$$

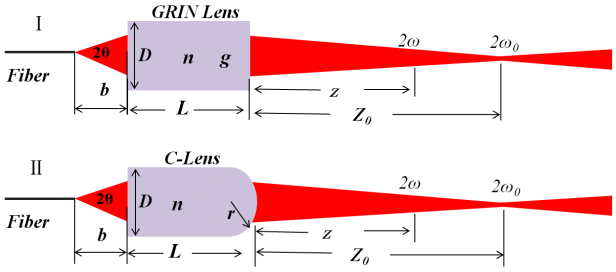

FIGURE 1. (I) The optical mode of fiber-coupling-focus module based on GRIN lens. (II) The optical mode of fiber-coupling-focus module based on C-lens.

In our design, the C-lens optical element is represented by an ABCD matrix, and the endoscopic probe system can be expressed by ABCD matrixes of all the elements. The C-lens ABCD matrix is expressed as:

$$T = \begin{bmatrix} 1 & 0 \\ \frac{1-n}{r} & n \end{bmatrix} \begin{bmatrix} 1 & L \\ 0 & 1 \end{bmatrix} \begin{bmatrix} 1 & 0 \\ 0 & \frac{1}{n} \end{bmatrix} = \begin{bmatrix} 1 & L\frac{1}{n} \\ \frac{1-n}{r} & \left[\frac{1-n}{r}L + n\right]\frac{1}{n} \end{bmatrix} \quad (2)$$

The ABCD matrix of position Z can be calculated as:

$$M = \begin{bmatrix} A & B \\ C & D \end{bmatrix} = \begin{bmatrix} 1 & z \\ 0 & 1 \end{bmatrix} T \begin{bmatrix} 1 & b \\ 0 & 1 \end{bmatrix} \quad (3)$$

$$q_0 = \frac{\pi k_0}{\lambda} i \quad (4)$$

$$q(b,z) = \frac{Aq_0 + B}{Cq_0 + D} \quad (5)$$

$$k(b,z) = \frac{1}{\sqrt{-\frac{\pi Im(\frac{1}{q(b,z)})}{\lambda}}} \quad (6)$$

$$R(b,z) = \frac{1}{Re(\frac{1}{q(b,z)})} \tag{7}$$

$$\omega_0(b) = \sqrt{\frac{k(b,z)^2}{1+\left[\frac{k(b,z)^2\pi}{R(b,z)\lambda}\right]^2}} \tag{8}$$

$$z_0(b) = \frac{R(b,z)}{1+\left[\frac{R(b,z)\lambda}{k(b,z)^2\pi}\right]^2} \tag{9}$$

III. RESULTS AND DISCUSSION

The parameter b is the assembled size, which can be adjusted during assembly and processing of the OCT catheter. However, the other three parameters (i.e.,*n, g,* and L for GRIN lenses, and n, r, and L for C-lens) are innate parameters of the optical lens and are fixed after processing.

Commercial GRIN lenses have a fixed central refractive index (n) and gradient constant (g). However, the length of the GRIN lens (L) can be cut and polished. Similarly, the distance between the fiber and the GRIN lens (b) can be adjusted during the assembling procedure. The design goal is that the working distance should be more than 10 mm with a spot size of the beam waist less 50 μm. Hence, the first numerical calculation shows the effects of b and L.

As shown in Fig. 1, the N.A. of the fiber is 0.14, corresponding to a divergence angle of θ. The diameter of the lens is 0.7 mm to control the size of the whole probe. b is limited by the diameter of the lens, which is the aperture of the whole optical system. The maximum beam diameter in the GRIN lens and the C-lens is limited to ~80% of the lens diameter. Therefore, the range of b is 0-2.5 mm, since the spot on the head surface is 0.5 mm when b = 2.5 mm.

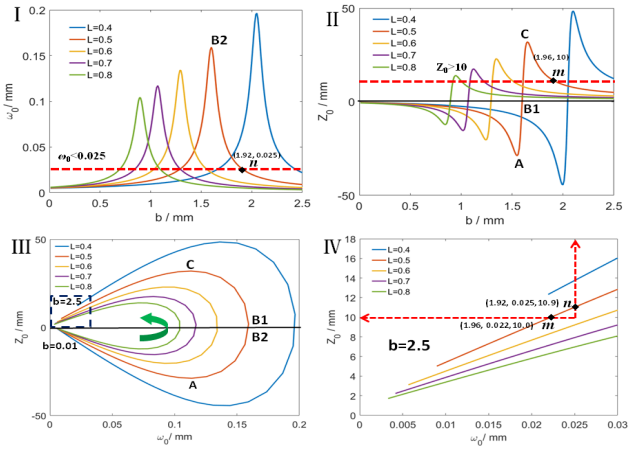

FIGURE 2. (I) The spot radius of catheter for varying b at different length of GRIN lens. (II) The working distance of the catheter for varying b at different length of GRIN lens. (III) Corresponding relationship between spot radius and working distance at different length of GRIN lens. (IV) The local zoom of (III). In this calculation, the parameters of GRIN lens are n = 1.6164 and g = 0.8521 mm^{-1}.

For a fixed GRIN lens, b will determine Z_0 and ω_0 of the output beam. Numerical simulations of a GRIN lens-based catheter are shown in Fig. 2, involving the effects of b and L. Fig. 2 (I) shows ω_0 at various b values from 0.01 mm to 2.5 mm with different color lines representing different lengths of the GRIN lens. The corresponding Z_0 is shown in Fig. 2 (II). In order to achieve a 10 mm working distance, the low pitch GRIN lens is selected. The central refractive index is 1.6164, and the gradient constant is 0.8521. The simulation shows five lengths of the GRIN lens (0.4 mm. 0.5 mm, 0.6 mm, 0.7 mm, and 0.8 mm). The greater GRIN lens lengths correspond to lower peak ω_0 and Z_0 values. From Fig. 2 (II), Z_0 <0 means that the beam waist is located to the left of the lens' rear surface. The 0.5 mm GRIN lens line is selected as a typical curve, and point A indicates that the beam waist is located at the left-most edge of the lens rear surface. Point B1 stands for the $Z_0 = 0$ condition, and the corresponding ω_0 has the greatest value (i.e., B2 in Fig. 2 (I)). Point C stands for the farthest beam waist. The designed requests are ω_0 <0.025 mm and Z_0 >10 mm. The red dashed line in Fig. 2 (I) means that $\omega_0 = 0.025$ mm, and the red dashed line in Fig. 2 (II) means that $Z_0 = 10$ mm. Hence, the designed parameters of b and Z_0 are restricted by the two dashed lines. For the typical curve ($L = 0.5$ mm) the critical points are n (1.92 mm, 0.025 mm) and m (1.96 mm, 10.0 mm), as shown in Fig. 2(I, II).

The relationship between Z_0 and ω_0 is shown in Fig. 2 (III) by synthesizing Fig. 2 (I) and Fig. 2 (II). The starting points of all curves correspond to $b = 0.01$ mm, and along the arrow direction, b increases to 2.5 mm at the end of each curve. The points A, (B1, B2) and C in Fig. 2 (I,II) can be contrasted to Fig. 2 (III), and points B1 and B2 are the same point in Fig. 2 (III), which is the crossover point of the curve line and the x-axis. Fig. 2 (IV) is a local zoom of Fig. 2 (III) to show more detail in the range of ω_0 from 0 mm to 0.03 mm. In Fig. 2 (IV), the arrow line in the horizontal direction represents the range of ω_0 <0.025 mm, and the arrow line in the vertical direction represents the range Z_0 >10 mm. The critical points n and m are also shown in Fig. 2 (IV). The parameters of (b, ω_0, Z_0) at point n are (1.92 mm, 0.025 mm, 10.9 mm) and at point m are (1.96 mm, 0.022 mm, 10.0 mm), which indicates that the adjustable range of b is 40 μm. Fig. 2 (IV) also indicates that the length of a GRIN lens has strong restrictions, since the 0.6 mm GRIN lens does not meet requirements and the 0.4 mm GRIN lens only partially meets the requirements. Therefore, the available length of a GRIN lens is confined to the range of 0.5±0.05 mm.

The same numerical calculation and analysis is performed for OCT catheter-based C-lenses, and the results are shown in Fig. 3. The radius of curvature of the rear surface (r) is −1.8 mm, and the refractive index (n) is 1.74. The lengths of the C-lenses are selected to be 2.0 mm, 2.5 mm, 3.0 mm, 3.5 mm and 4.0 mm. Fig. 3 (I,II) shows the ω_0 and Z_0 values at various b values from 0.01 mm to 2.5 mm with different L values. It is interesting that the shape of all curves at different lens lengths is the same, and the only difference is that these curves translate at the abscissa. The curve of the 0.5 mm GRIN lens is selected as a typical curve. The critical points for the C-lens catheter are n (1.19 mm, 0.025 mm, 14.5 mm) and m

(1.48 mm, 0.016 mm, 10.0 mm), which indicates that the adjustable range of b is 300 μm. All five lengths of the C-lens meet the design requirements. The calculated results indicate that the assembling tolerance of a C-lens is much higher than that of a GRIN lens. Furthermore, the available length of a C-lens is much longer than that of a GRIN lens.

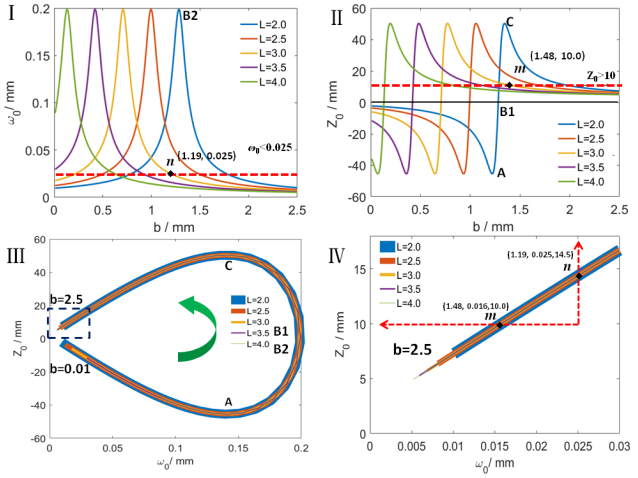

FIGURE 3. **(I) The spot radius of catheter for varying b at different length of C-lens. (II) The working distance of the catheter for varying b at different length of C-lens. (III) Corresponding relationship between spot radius and working distance at different length of C-lens. (IV) The local zoom of (III). The parameters of C-lens are n = 1.74 mm and r = −1.8 mm.**

Fig. 4 shows the effects of the lenses' lengths on ω_0 and Z_0. The previous analysis has pointed out the ranges for the guiding parameters for meeting the design requirements. In this simulation, the parameters of the GRIN lens are listed as follows: $n = 1.6164$, $g = 0.8521$ mm^{-1}, $b = 1.95$ and $L = 0.4$-0.6 mm. The parameters of the GRIN lens are $n = 1.74$, $r = -1.8$ mm, $b = 1.20$ and $L = 2.0$-4.0 mm. Fig. 4(I) shows the spot radius at various L values of the GRIN lens and the C-lens. Although the lengths of the GRIN lens and the C-lens are located in different ranges, ω_0 has a similar range. Fig. 4(III) shows the sensitivity of the spot radius with L, but the x coordinate is labeled with ω_0 by changing the L value to the corresponding spot radius. The sensitivity is the differential of the lines in Fig. 4(I). Similarly, Fig. 4 (II, IV) shows the working distance and its sensitivity to L. The green dashed line in Fig. 4 (I) stands for $\omega_0 = 0.03$ mm, while the dashed line in Fig. 4 (II) stands for $Z_0 = 15$ mm, and the sensitivity is focused on the range of $\omega_0 < 0.03$ mm and $Z_0 < 15$ mm. The critical points are marked as ω_G and Z_G for the GRIN lens and ω_C and Z_C for the C-lens. As shown in Fig. 4(III), the sensitivity of ω_0 *Vs* L for the GRIN lens is 0.207 mm/mm at $\omega_0 = 0.02$ mm, which indicates that the longitudinal tolerance of the GRIN lens should be less than 5 μm to ensure that the tolerance of ω_0 is less than 1 μm. For the C-lens, the sensitivity is 0.018 mm/mm, so the tolerance can be expanded to 55 μm to ensure the same tolerance of ω_0. As shown in Fig. 4(IV), the sensitivity of Z_0 *Vs* L for the GRIN lens is 24 times higher than that of the C-lens. The sensitivity of the C-lens is 5 mm/mm at $Z_0 = 10$ mm, which indicates that the longitudinal tolerance of the C-lens must be 200 μm to ensure that the tolerance of Z_0 is less than 1 mm. However, the value decreases to 8.3 μm to achieve the same precision for the GRIN lens. A processing precision of hundreds of micrometers is easily achieved; however, several micrometers is difficult to realize.

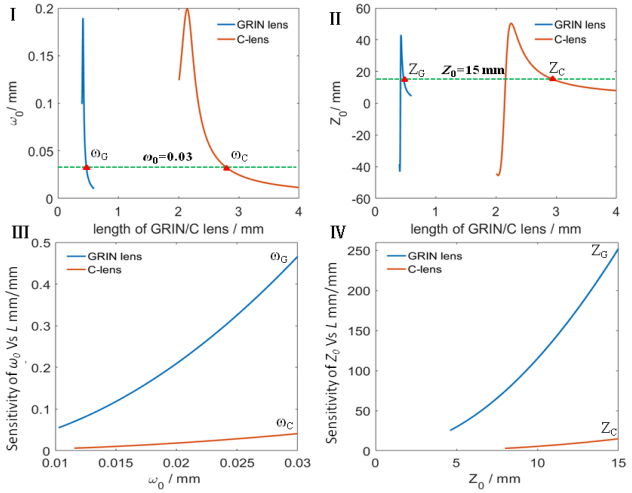

FIGURE 4. **(I) The spot radius of OCT catheter for the length of GRIN lens and C-lens. (II) The working distance of OCT catheter for the length of GRIN lens and C-lens. (III) The sensitivity of spot radius to the length of GRIN lens and C-lens. (IV) The sensitivity of working distance to the length of GRIN lens and C-lens.**

A similar analysis has been performed to determine the effect of the radius of curvature of a C-lens, and the results are shown in Fig. 5. A radius of curvature less than −1.2 mm meets the design requirements, which indicates that the tolerance for the radius of curvature is good enough. The radius of curvature is also dependent on the processing size, so the sensitivity of the radius of curvature of a C-lens is compared with the sensitivity of the length of a GRIN lens. The results are shown in Fig. 6. The sensitivity of the length of a GRIN lens is approximately five times larger than the sensitivity of the radius of curvature for a C-lens.

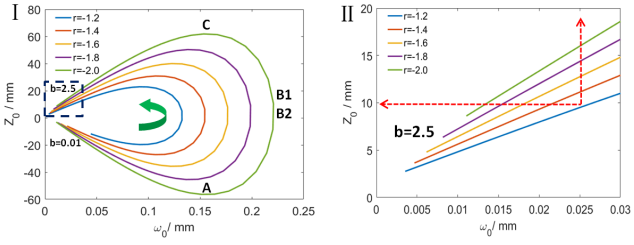

FIGURE 5. **(I) Corresponding relationship between spot radius and working distance at different curvature radius of C-lens. (II) The local zoom of (I). In this calculation, the parameters of C-lens are n = 1.74 and L = 3.0 mm.**

The same analysis has been performed regarding the assembling precision (i.e., the sensitivity to ω_0 *Vs* b and Z_0 *Vs* b). ω_0 and Z_0 at various b values are shown

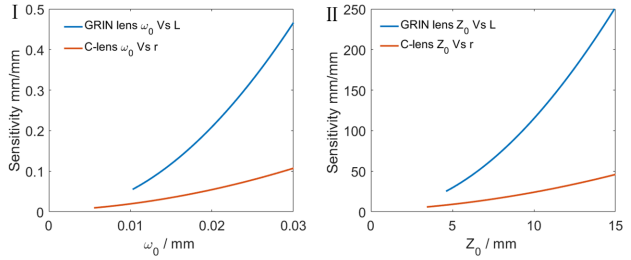

FIGURE 6. The sensitivity of ω_0 Vs L for GRIN lens and ω_0 Vs r for C-lens. (II) The sensitivity of Z_0 Vs L for GRIN lens and Z_0 Vs r for C-lens.

in Fig. 7(I,II), and the sensitivities of ω_0 *Vs b* and Z_0 *Vs b* are shown in Fig. 7 (III,IV). In this simulation, the parameters of the GRIN lens are listed as follows: n = 1.6164, g = 0.8521 mm^{-1}, $L = 0.5$ mm and $b = 0.01$-2.5 mm. The most commonly used C-lens is selected for the simulation, and the parameters of the C-lens are listed as follows: $n = 1.74$, $r = -1.8$ mm, $L = 3.0$ mm and $b = 0.01$-2.5 mm. The results show that the sensitivity of the GRIN lens is about twice as high as that of the C-lens. There is not a great difference in the sensitivity to the assembling precision between the GRIN lens probe and the C-lens probe.

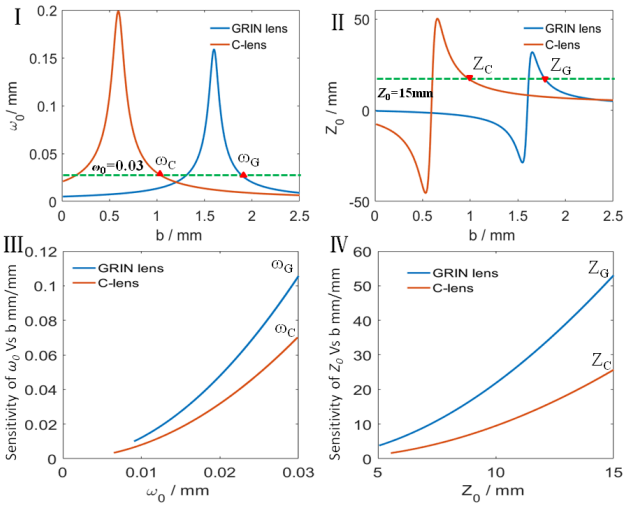

FIGURE 7. (I) The spot radius of OCT catheter for varying b of GRIN lens and C-lens. (II) The working distance of OCT catheter for varying b of GRIN lens and C-lens. (III) The sensitivity of the spot radius to *b* of GRIN lens and C-lens. (IV) The sensitivity of working distance to *b* of GRIN lens and C-lens.

The effect of the refractive index is also analyzed in both GRIN lenses and C-lenses. The effect of the central refractive index of both GRIN lenses and C-lenses is shown in Fig. 8. All the refractive indexes meet the design requirements. Hence, the tolerance of the refractive index is large enough for both GRIN lenses and C-lenses, and the sensitivity is low.

The effect of the gradient constant of the GRIN lens is shown in Fig. 9. In this calculation, the parameters of the GRIN lens are listed as follow: $n = 1.6164$, $L = 3.0$ mm and $b = 0.01$-2.5 mm. The results show that $g = 0.80$ and $g = 0.85$ meet the design requirements.

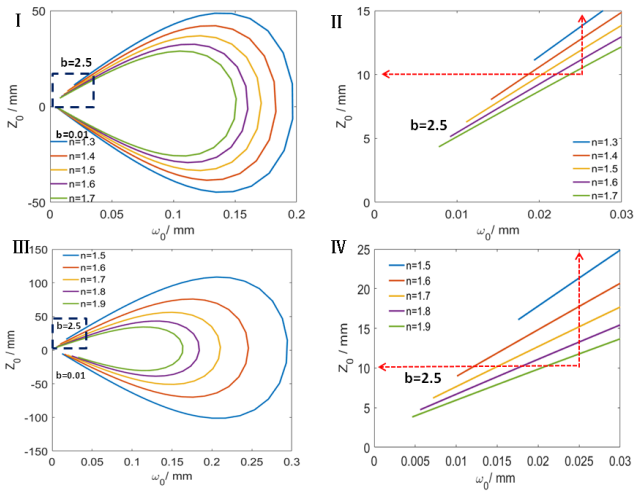

FIGURE 8. (I) Corresponding relationship between spot radius and working distance at different refractive index of GRIN lens. (II) The local zoom of (I). The parameters of GRIN lens are g = 0.853 mm and L = 0.5 mm. (III) corresponding relationship between spot radius and working distance at different refractive index of C-lens. (IV) The local zoom of (III). In this calculation, the parameters of C-lens are r = −1.8 mm and L = 3.0 mm.

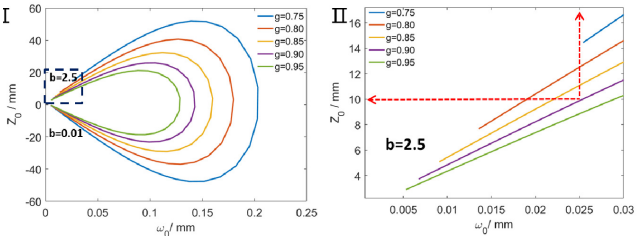

FIGURE 9. The corresponding relationship between spot radius and working distance at different gradient constant of GRIN lens. (II) The local zoom of (I). The parameters of GRIN lens are L = 0.5 mm, n = 1.6164.

The ABCD matrix calculation method has very small errors because the C-lens is thick. As shown in Fig. 10 (I), Zemax is used to simulate the optical model of the C-lens catheter. The design parameters are listed as follows: $b = 1.4$ mm, $L = 3.2$ mm, $r = -1.8$ mm, and the glass is selected to be N-LAF3, whose refractive index is approximately 1.74. The distance between the imaging surface and the C-lens' rear surface is 11.2 mm. The result from Zemax shows that the geometrical radius of the spot is 14.0 μm. The root-mean-square (RMS) radius is 9.4 μm, and the airy diameter is 19.08 μm. The modulation transfer function (MTF) of the C-lens catheter is shown in Fig. 10 (II), and the MTF curve (blue line) well approximates the diffraction limit curve (black line). Therefore, this catheter will present good image performance.

According to the Zemax simulation, we construct an OCT catheter based on a C-lens. The beam analysis and results of the C-lens probe are shown in Fig. 11. A beam analyzer (Thorlabs, BP209-IR) is used to test the width of the beam at different distances, as shown in Fig. 11 (I). The Z direction is the beam propagation direction, the X direction is the

horizontal direction, and the Y direction stands for the vertical direction. Fig. 11 (I, II) shows the beam profile of XOZ and YOZ at different distances. The $1/e^2$ of the peak power is considered to be the beam width, as is shown with the red dashed line. The width of the beam at different locations is shown in Fig. 10 (IV), which indicates that the beam waist is located at 11 mm and the diameter is 41 μm.

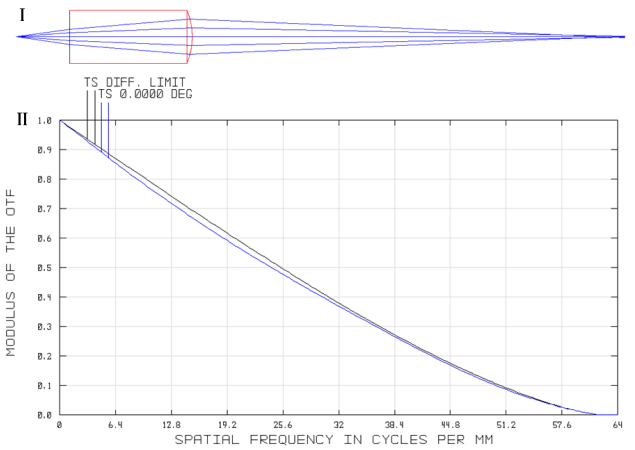

FIGURE 10. (I) The Zemax optical model of C-lens catheter. (II) The MTF curve.

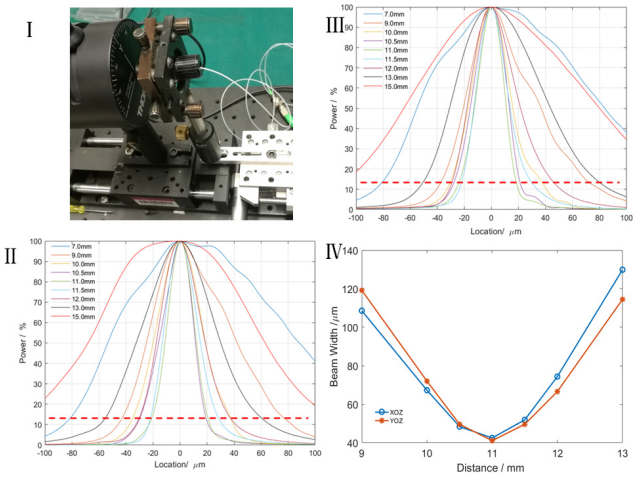

FIGURE 11. (I) The beam quality testing setup. (II) The XOZ profile of the beam. (III) The YOZ profile of the beam. (IV) The beam diameter changing along the propagation direction.

Comparisons of the sensitivity between the GRIN lens and the C-lens are listed as follows (Tab. 1 and Tab. 2).

The sensitivity of the C-lens is 5 mm/mm at $Z_0 = 10$ mm, which indicates that the longitudinal tolerance of the C-lens must be 200 μm to ensure that the tolerance of Z_0 is less than 1 mm. However, the value decreases to 8.3 μm to achieve the same level of precision for the GRIN lens. A processing precision of hundreds of micrometers is easily achieved; however, several micrometer processing precision is difficult to realize.

As the validation of the theoretical calculation, the actual images based on GRIN lens also been acquired in previous research. The working distance is usually less than 6 mm as

TABLE 1. The sensitivity of GRIN lens and C-lens.

	Sensitivity of GRIN lens	Sensitivity of C-lens
ω_0 Vs L (mm/mm) (at ω_0=20 μm)	0.207	0.018
ω_0 Vs b (mm/mm) (at ω_0=20 μm)	0.048	0.030
ω_0 Vs n (at ω_0=20 μm)	0.060	0.106
ω_0 Vs r (mm/mm) (at ω_0= 20 μm)	——	0.552
Z_0 Vs L (mm/mm) (at Z_0=10 mm)	120.5	5.0
Z_0 Vs b (at Z_0=10 mm) (mm/mm)	21.8	9.4
Z_0 Vs n (at Z_0=10 mm)	33.5	45
Z_0 Vs r (at Z_0=10 mm) (mm/mm)	——	24.7

TABLE 2. The ratio of sensitivity of GRIN lens and C-lens.

Sensitivity of GRIN lens	Sensitivity of C-lens	ratio
ω_0 Vs L	ω_0 Vs L	11
ω_0 Vs L	ω_0 Vs r	4
Z_0 Vs L	Z_0 Vs L	24
Z_0 Vs L	Z_0 Vs r	5
ω_0 Vs b	ω_0 Vs b	2
Z_0 Vs b	Z_0 Vs b	2
ω_0 Vs n	ω_0 Vs n	1
Z_0 Vs n	Z_0 Vs n	1

mentioned earlier [14]. The OCT probe based on the elaborately manufactured GRIN lens can reach approximately 10 mm working distance [25]. Similarly, the actual images has been acquired the images of the endoscopic OCT based on C-lens described as our previous research [26], [27]. The working distance is approximate 10 mm for imaging the biological tissue. The GRIN lens-based endoscopic OCT probes have high-performance imaging effect in the short working distance. As mentioned above, the fabricated probe in early stage is usually considered as working in a small space, such as intravascular. Furthermore, the GRIN lens is a good choice for proximally driving scanning, because the flat end face of GRIN lenses is easily combined with the prism. GRIN lens is usually and widely used into endoscopic OCT probes. Lastly, the current clinical application aims to image the large-scale space, the working distance is usually large (∼10 mm), such as imaging the digestive tract [17], [18]. Hence, a long-working-distance probe is important. Due to the low cost and the good imaging performance, the C lens-based endoscopic probe is a better choice for imaging the large-scale working space.

IV. CONCLUSION

For miniaturized OCT probes, the GRIN lens is extensively designed, as has been previously reported. A GRIN lens is the best choice for a catheter with a short working distance, which has been proved by many of studies. However, it is a great challenge to fabricate a probe with a greater than 10 mm working distance probe using a GRIN lens. In this paper, we perform an extensive and elaborate comparison of the long working distance probes using GRIN lenses and C-lenses. There are four parameters that affect the output beam (i.e.,ω_0 and Z_0). The assembling size is b, the processing size includes L and r for C-lenses and L for GRIN lenses, and the optical

parameters involve n for C-lenses and n and g for GRIN lenses. Our calculations suggest that a C-lens is a better choice for long-working-distance OCT probes.

ACKNOWLEDGMENT

(Yingwei Fan and Site Luo contributed equally to this work.)

REFERENCES

[1] D. Huang, E. A. Swanson, C. P. Lin, J. S. Schuman, W. G. Stinson, W. Chang, M. R. Hee, T. Flotte, K. Gregory, and C. A. Puliafito, "Optical coherence tomography," *Science*, vol. 254, no. 5035, pp. 1178–1181, 1991.

[2] Y. Fan, L. Ma, W. Jiang, S. Luo, X. Zhang, and H. Liao, "Optimized optical coherence tomography imaging with Hough transform-based fixed-pattern noise reduction," *IEEE Access.*, vol. 6, pp. 32087–32096, 2018.

[3] G. J. Tearney, M. E. Brezinski, B. E. Bouma, S. A. Boppart, C. Pitris, J. F. Southern, and J. G. Fujimoto, "*In vivo* endoscopic optical biopsy with optical coherence tomography," *Science*, vol. 276, no. 5321, pp. 2037–2039, Jun. 1997.

[4] Y. Mao, S. Chang, S. Sherif, and C. Flueraru, "Graded-index fiber lens proposed for ultrasmall probes used in biomedical imaging ," *Appl. Opt.*, vol. 46, no. 23, pp. 5887–5894, Aug. 2007.

[5] P. R. Herz, Y. Chen, A. D. Aguirre, J. G. Fujimoto, H. Mashimo, J. Schmitt, A. Koski, J. Goodnow, and C. Petersen, "Ultrahigh resolution optical biopsy with endoscopic optical coherence tomography," *Opt. Express*, vol. 12, no. 15, pp. 3532–3542, Jul. 2004.

[6] P. H. Tran, D. S. Mukai, M. Brenner, and Z. Chen, "*In vivo* endoscopic optical coherence tomography by use of a rotational microelectromechanical system probe," *Opt. Lett.*, vol. 29, no. 11, pp. 1236–1238 Dec. 2004.

[7] N. Zhang, T.-H. Tsai, O. O. Ahsen, K. Liang, H.-C. Lee, P. Xue, X. Li, and J. G. Fujimoto, "Compact piezoelectric transducer fiber scanning probe for optical coherence tomography," *Opt. Lett.*, vol. 39, no. 2, pp. 186–188 Jan. 2014.

[8] A. Jain, A. Kopa, Y. Pan, G. K. Fedder, and H. Xie, "A two-axis electrothermal micromirror for endoscopic optical coherence tomography," *IEEE J. Sel. Topics Quantum Electron.*, vol. 10, no. 3, pp. 636–642, May 2004.

[9] C. Duan, Q. Tanguy, A. Pozzi, and H. Xie, "Optical coherence tomography endoscopic probe based on a tilted MEMS mirror," *Biomed. Opt. Express*, vol. 7, no. 9, pp. 3345–3354, Aug. 2016.

[10] D. L. Wang, L. L. Fu, X. Wang, Z. J. Gong, S. Samuelson, C. Duan, H. Z. Jia, J.-S. Ma, and H. Xie, "Endoscopic swept-source optical coherence tomography based on a two-axis microelectromechanical system mirror," *Proc. SPIE*, vol. 18, no. 8. Aug. 2013, Art. no. 086005.

[11] W. G. Jung, D. T. McCormick, Y.-C. Ahn, A. Sepehr, M. Brenner, B. Wong, N. C. Tien, and Z. P. Chen, "*In vivo* three-dimensional spectral domain endoscopic optical coherence tomography using a microelectromechanical system mirror," *Opt. Lett.*, vol. 32, no. 22, pp. 3239–3241, Oct. 2007.

[12] J. Sun, S. Guo, L. Wu, L. Liu, S.-W. Choe, B. S. Sorg, and H. Xie, "3D *in vivo* optical coherence tomography based on a low-voltage, large-scan-range 2D MEMS mirror," *Opt. Express*, vol. 18, no. 12, pp. 12065–12075, May 2010.

[13] K. H. Kim, B. H. Park, G. N. Maguluri, T. W. Lee, F. J. Rogomentich, M. G. Bancu, B. E. Bouma, J. F. de Boer, and J. J. Bernstein, "Two-axis magnetically-driven MEMS scanning catheter for endoscopic high-speed optical coherence tomography," *Opt. Express*, vol. 15, no. 26, pp. 18130–18140, Dec. 2007.

[14] C. Duan, J. Sun, S. Samuelson, and H. Xie, "Probe alignment and design issues of microelectromechanical system based optical coherence tomography endoscopic imaging," *Appl. Opt.*, vol. 52, no. 26, pp. 6589–6598, Sep. 2013.

[15] M. V. Sivak, K. Kobayashi, J. A. Izatt, A. M. Rollins, R. Ung-Runyawee, A. Chak, R. C. Wong, G. A. Isenberg, and J. Willis, "High-resolution endoscopic imaging of the GI tract using optical coherence tomography," *Gastrointestinal Endoscopy*, vol. 51, no. 4, pp. 474–479, Apr. 2000.

[16] S. Jäckle, N. Gladkova, F. Feldchtein, A. Terentieva, B. Brand, G. Gelikonov, V. Gelikonov, A. Sergeev, A. Fritscher-Ravens, J. Freund, U. Seitz, S. Schröder, and N. Soehendra, "*In Vivo* endoscopic optical coherence tomography of esophagitis, Barrett's esophagus, and adenocarcinoma of the esophagus," *Endoscopy*, vol. 32, no. 10, pp. 750–755, Oct. 2000.

[17] X. D. Li, S. A. Boppart, J. Van Dam, H. Mashimo, M. Mutinga, W. Drexler, M. Klein, C. Pitris, M. L. Krinsky, M. E. Brezinski, and J. G. Fujimoto, "Optical coherence tomography: Advanced technology for the endoscopic imaging of Barrett's esophagus," *Endoscopy*, vol. 32, no. 12, pp. 921–930, Dec. 2000.

[18] M. J. Gora, M. J. Suter, G. J. Tearney, and X. Li, "Endoscopic optical coherence tomography: Technologies and clinical applications [Invited]," *Biomed. Opt. Express*, vol. 8, no. 5, pp. 2405–2444, 2017.

[19] B. J. Vakoc, M. Shishko, S. H. Yun, W. Y. Oh, M. J. Suter, A. E. Desjardins, J. A. Evans, N. S. Nishioka, G. J. Tearney, and B. E. Bouma, "Comprehensive esophageal microscopy by using optical frequency—Domain imaging (with video)," *Gastrointestinal Endoscopy*, vol. 65, no. 6, pp. 898–905, May 2007.

[20] M. J. Suter, B. J. Vakoc, P. S. Yachimski, M. Shishkov, G. Y. Lauwers, M. Mino-Kenudson, B. E. Bouma, N. S. Nishioka, and G. J. Tearney, "Comprehensive microscopy of the esophagus in human patients with optical frequency domain imaging," *Gastrointestinal Endoscopy*, vol. 68, no. 4, pp. 745–753, Oct. 2008.

[21] W. Kang, H. Wang, Y. S. Pan, M. W. Jenkins, G. A. Isenberg, A. Chak, M. Atkinson, D. Agrawal, Z. L. Hu, and A. M. Rollins, "Endoscopically guided spectral-domain OCT with double-balloon catheters," *Opt. Express*, vol. 18, no. 16, pp. 17364–17372, Aug. 2010.

[22] T. S. Wang, A. F. W. van der Steen, and G. van Soest, "Numerical analysis of astigmatism correction in gradient refractive index lens based optical coherence tomography catheters," *Appl Opt.*, vol. 51, no. 21, pp. 5244–5252, Jul. 2012.

[23] W. Jung, W. Benalcazar, A. Ahmad, U. Sharma, H. Tu, and S. A. Boppart, "Numerical analysis of gradient index lens-based optical coherence tomography imaging probes," *J. Biomed. Opt.*, vol. 15, no. 6, Oct. 2010, Art. no. 066027.

[24] H. L. Fu, Y. X. Leng, M. J. Cobb, K. Hsu, J. H. Hwang, and X. D. Li, "Flexible miniature compound lens design for high-resolution optical coherence tomography balloon imaging catheter," *J. Biomed. Opt.*, vol. 13, no. 6. Dec. 2008, Art. no. 060502.

[25] J. F. Xi, L. Huo, Y. C. Wu, M. J. Cobb, J. H. Hwang, and X. D. Li, "High-resolution OCT balloon imaging catheter with astigmatism correction," *Opt. Lett.*, vol. 34, no. 13, pp. 1943–1945, Jul. 2009.

[26] S. Luo, L. Zhou, D. Wang, C. Duan, H. Liu, Y. Zhu, G. Li, H. Zhao, J. Tang, Y. Wu, X. An, X. Li, Y. Liu, H. Xie, and L. Huo, "A miniature endoscopic optical coherence tomography probe based on C-lens," *IEEE Photon. J.*, vol. 10, no. 5, pp. 1–10, Oct. 2018.

[27] S. Luo, D. Wang, J. Tang, L. Zhou, C. Duan, D. Wang, H. Liu, Y. Zhu, G. Li, H. Zhao, Y. Wu, X. An, X. Li, Y. Liu, L. Huo, and H. Xie, "Circumferential-scanning endoscopic optical coherence tomography probe based on a circular array of six 2-axis MEMS mirrors," *Biomed. Opt. Express*, vol. 9, pp. 2104–2114, May 2018.

[28] H. Pahlevaninezhad, M. Khorasaninejad, Y.-W. Huang, Z. Shi, L. P. Hariri, D. C. Adams, V. Ding, A. Zhu, C.-W. Qiu, F. Capasso, and M. J. Suter, "Nano-optic endoscope for high-resolution optical coherence tomography *in vivo*," *Nature Photon.*, vol. 12, pp. 540–547, Jul. 2018.